Acta Crystallographica Section D
Biological Crystallography
ISSN 0907-4449

Structure of an orthorhombic form of xylanase II from *Trichoderma reesei* and analysis of thermal displacement

Nobuhiko Watanabe,‡ Toshihiko Akiba, Ryuta Kanai§ and Kazuaki Harata*

Biological Information Research Center, National Institute of Advanced Industrial Science and Technology (AIST), Central 6, 1-1-1 Higashi, Tsukuba, Ibaraki 305-8566, Japan

‡ Present address: Department of Biochemistry, 429 Medical Sciences Building, University of Alberta, Edmonton, AB T6G 2H7, Canada.
§ Present address: Department of Molecular Physics and Biochemistry, Yale University, 266 Whitney Avenue, Bass 431, New Haven, CT 06520-8114, USA.

Correspondence e-mail: k-harata@aist.go.jp

Received 2 March 2006
Accepted 11 May 2006

PDB References: xylanase II, 100 K, 2dfb, r2dfbsf; 293 K, 2dfc, r2dfcsf.

An orthorhombic crystal of xylanase II from *Trichoderma reesei* was grown in the presence of sodium iodide. Crystal structures at atomic resolution were determined at 100 and 293 K. Protein molecules were aligned along a crystallographic twofold screw axis, forming a helically extended polymer-like chain mediated by an iodide ion. The iodide ion connected main-chain peptide groups between two adjacent molecules by an N—H···I^-···H—N hydrogen-bond bridge, thus contributing to regulation of the molecular arrangement and suppression of the rigid-body motion in the crystal with high diffraction quality. The structure at 293 K showed considerable thermal motion in the loop regions connecting the β-strands that form the active-site cleft. TLS model analysis of the thermal motion and a comparison between this structure and that at 100 K suggest that the fluctuation of these loop regions is attributable to the hinge-like movement of the β-strands.

1. Introduction

Proteins are dynamic molecules having non-rigid but flexible structures that fluctuate even in the crystalline state (Artymiuk *et al.*, 1979; Doucet & Benoit, 1987; Zhang *et al.*, 1995; Petsko, 1996; DePristo *et al.*, 2004). Structural changes in functional domains or groups have been widely observed when proteins bind substrates, ligands or other proteins. Therefore, knowledge of molecular flexibility and dynamics is essential for understanding protein activity. In crystal structures, the mobility of protein molecules is represented in terms of atomic displacement parameters (ADPs). Since anisotropic ADPs contain information on not only the magnitude of atomic vibration but also the direction of atomic movement (Merritt, 1999), analysis of anisotropic ADPs is expected to provide information about the dynamic properties of proteins related to their function (Sternberg *et al.*, 1979; Harata *et al.*, 1999; Harata & Kanai, 2002; Matoba & Sugiyama, 2003). In the crystal structure determination of proteins, isotropic ADPs, which correspond to the magnitude of atomic vibration, are usually adopted because of a poor data-to-parameter ratio resulting from the limited resolution of observed diffraction data. The use of anisotropic ADPs is generally accepted in structure analyses at atomic resolutions above 1.2 Å.

It is well known that the addition of some minor chemical components to the crystallization solution improves the diffraction quality of crystals (Bergfors, 1999; Ducruix & Giegé, 1999; McPherson, 1999). The binding of additive compounds to protein molecules is expected to suppress the fluctuation of protein structures or to strengthen intermolecular contacts to form better crystal packing. We have

been screening for good additives for several proteins in order to grow crystals that diffract to atomic resolution. In the crystallization of xylanase II from *Trichoderma reesei*, we found that the addition of sodium iodide to the crystallization solution induced the growth of a new crystal that diffracted to 1.1 Å resolution. This high-resolution crystal enabled us to analyze the thermal motion of the protein using anisotropic ADPs.

Xylanase II is an enzyme classified into glycoside hydrolase family 11 (Henrissat & Bairoch, 1993). It catalyzes the hydrolysis of the β-1,4-linkage of xylosides. Crystal structures and molecular-dynamics simulation of xylanase II have suggested the presence of a hinge motion of the structural elements at the active-site cleft (Törrönen & Rouvinen, 1995; Muilu *et al.*, 1998). However, the structural change upon substrate binding is small in xylanases from *Bacillus agaradhaerens* (Sabini *et al.*, 1999) and *B. circulans* (Wakarchuk *et al.*, 1994; Sidhu *et al.*, 1999). Atomic resolution structures deposited in the Protein Data Bank (http://www.rcsb.org/pdb/) have mostly been determined at temperatures around 100 K (Schmidt & Lamzin, 2002). In addition, several reports have compared the structural properties at atomic resolution between structures determined at low temperature near 100 K and at non-freezing temperatures (Walsh *et al.*, 1998; Usón *et al.*, 1999; Teeter *et al.*, 2001). An atomic resolution structure of the family 11 xylanase from *B. agaradhaerens* determined at 120 K has been reported (Sabini *et al.*, 2001). In this paper, we present the crystal structures of xylanase II at atomic resolution and discuss the fluctuation of the protein structure based on ADP analysis using the TLS model (Schomaker & Trueblood, 1968). In addition, we present a comparison of the structures determined at 100 K and 293 K.

Table 1
Statistics of data collection and summary of structure determination.

Temperature (K)	100	293	290
Crystal data			
Space group	$P2_12_12_1$		
Z	4		
Unit-cell parameters			
a (Å)	48.97	49.55	49.55
b (Å)	58.51	60.03	60.08
c (Å)	69.80	70.50	70.50
V_M (Å^3 Da^{-1})	2.5	2.5	2.5
Data collection			
Wavelength (Å)	1.15	1.15	1.5418
Resolution range (Å)	19.8–1.11 (1.17–1.11)	20.0–1.19 (1.26–1.19)	20.0–1.28 (1.35–1.28)
No. of observations	514163 (62611)	464161 (64014)	311226 (15881)
No. of unique data	77541 (9975)	67093 (9724)	52045 (6270)
Multiplicity	6.6 (6.3)	6.9 (6.6)	6.0 (2.5)
Completeness (%)	96.9 (86.5)	99.2 (99.6)	94.9 (79.9)
R_{merge}	0.066 (0.203)	0.046 (0.392)	0.064 (0.360)
Structure refinement			
Resolution range (Å)	19.8–1.11 (1.16–1.11)	20.0–1.19 (1.24–1.19)	20.0–1.37 (1.43–1.37)
No. of reflections	77502 (7691)	67084 (7039)	42436 (4181)
No. of parameters	16689	15375	15321
R value for all data	0.108 (0.108)	0.106 (0.150)	0.127 (0.293)
R_{free} value for 5% of data	0.121	0.122	0.171
Maximum residual density (positive/negative) (e Å^{-3})	0.34/−0.33	0.30/−0.56	0.32/−0.29
Contents of the asymmetric unit			
Protein molecules	1	1	1
Sulfate-ion sites	1	0	0
Iodide-ion sites	6	1	1
Water sites	348	208	196
Average coordinate error (Å)			
Main-chain atoms	0.009	0.013	0.020
All atoms	0.021	0.022	0.030

2. Materials and methods

2.1. Preparation of orthorhombic crystals

Xylanase II (endo-1,4-β-xylanase II; EC 3.2.1.8) from *T. reesei* was purchased from Hampton Research (Laguna Niguel, CA, USA) in a solution form. Prior to the crystallization experiments, an aliquot of the protein solution (~33 mg ml^{-1}) was dialyzed overnight against 10 m*M* bicine buffer pH 9.0 containing 1 m*M* magnesium sulfate and 1 m*M* DTT (dithiothreitol) and was subsequently filtered through a 0.22 µm Ultrafree-MC filter (Millipore, Billerica, MA, USA). The protein concentration of the filtrate was determined with a BCA protein-assay kit (Pierce, Rockford, IL, USA) and was adjusted to 20 mg ml^{-1}.

The sitting-drop vapour-diffusion method was employed for crystallization. Drops of 4 µl in volume were prepared by mixing 2 µl protein solution, 0.6 µl 1 *M* sodium iodide and 1.4 µl reservoir solution (1.2–1.3 *M* ammonium sulfate, 100 m*M* bicine pH 9.0). Each drop was then equilibrated with 50–100 µl reservoir solution at 298 K. In fewer than a quarter of the drops prepared, crystals of the protein appeared within 4–5 d. To overcome this low success rate, microseeding was routinely performed. Seed crystals were prepared by crushing several pieces of the crystal in 50 µl reservoir solution containing 150 m*M* sodium iodide using a Seed Bead kit (Hampton Research). 2 µl of the seed stock, diluted 10^{-3}–10^{-5} with the same solution, was mixed with an equal volume of the protein solution to make a sitting drop, which was then equilibrated with the same reservoir solution. Crystals began appearing the next day and grew to as large as 0.3–0.5 mm in a week. The seeding assured that these large crystals were obtained from more than 90% of the drops.

2.2. Data collection

Data sets were collected at 290 K from a crystal sealed in a glass capillary on a Bruker SMART6000 diffractometer with Cu $K\alpha$ radiation from a MAC Science M06X rotating-anode generator (50 kV, 90 mA, focal spot size 0.3 mm) equipped

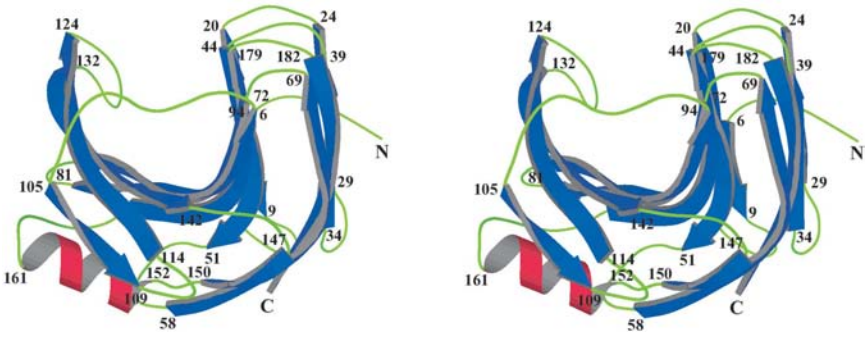

Figure 1
A stereoscopic view of the structure of xylanase II drawn using *MOLSCRIPT* (Kraulis, 1991).

with Osmic Confocal MaxFlux Optics (Osmic, Auburn Hills, MI, USA). Diffraction data were indexed and integrated with *SMART* and *SAINT*+ (Bruker AXS, Madison, WI, USA). Subsequent data scaling and reduction to structure-factor amplitudes were performed with *SCALA* (Evans, 1993) and *TRUNCATE* (French & Wilson, 1978) from the *CCP*4 program suite (Collaborative Computational Project, Number 4, 1994).

Data sets were also collected at 100 and 293 K on beamline BL-18B at the Photon Factory (KEK, Tsukuba, Japan) using an ADSC Quantum 4R CCD detector. For data collection at 100 K, crystals were flash-frozen in a cryocooled nitrogen-gas stream after being briefly dipped in reservoir solution supplemented with 20%(*w*/*v*) glycerol. The recorded diffraction patterns were processed by *HKL*2000 (Otwinowski & Minor, 1997) and reduced to structure-factor amplitudes by *TRUNCATE*. Statistics of these data sets calculated with *SCALA* are summarized in Table 1.

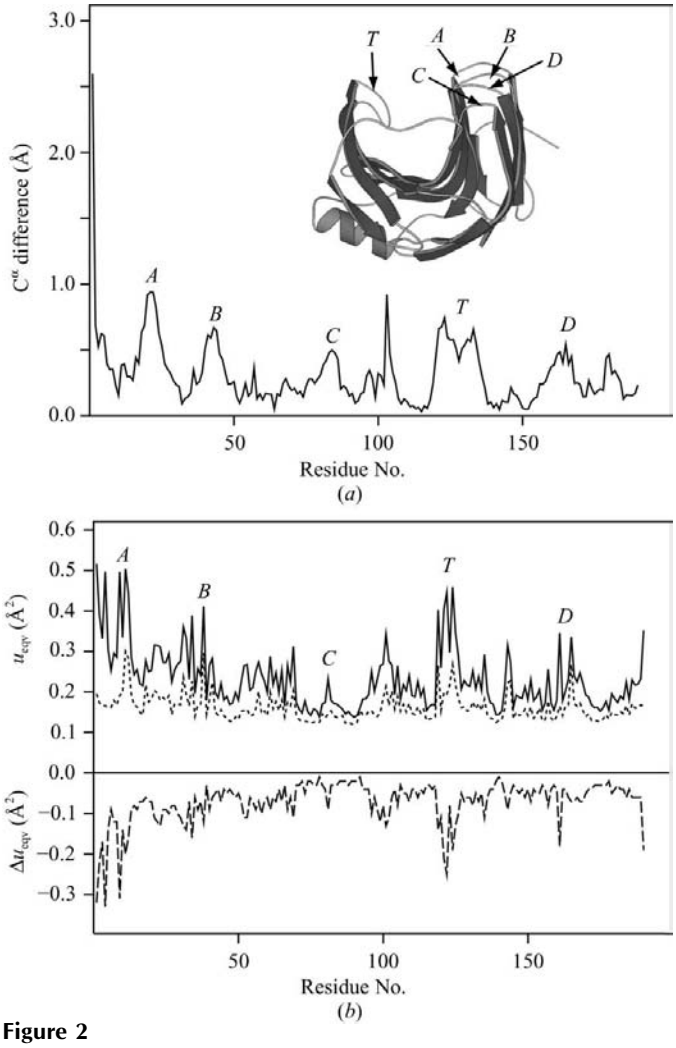

Figure 2
Comparison of the backbone structure and equivalent isotropic displacement parameters between the structures at 100 and 293 K. Differences between equivalent C^{α} atoms (*a*) were calculated after the least-squares superposition of the two structures. Loop regions corresponding to the five 'fingertips' are denoted *A*, *B*, *C*, *D* and *T*. The average u_{eqv} values for the amino-acid residues in the structures at 293 and 100 K are plotted by a solid line and dotted line (*b*), respectively. Δu_{eqv} is calculated as $\Delta u_{eqv} = u_{eqv}(100\ \mathrm{K}) - u_{eqv}(293\ \mathrm{K})$.

2.3. Structure determination and refinement

The crystal structure at 290 K was determined by molecular replacement using the program *CNS* (Brünger *et al.*, 1998) and the atomic coordinates of the xylanase II structure from a monoclinic crystal (PDB code 1enx; Törrönen *et al.*, 1994). The structures at 100 and 293 K were determined by the same procedure using the coordinates of the refined 290 K structure. The structures were refined by the full-matrix least-squares method using the program *SHELX*97 (Sheldrick, 1997). H-atom coordinates were calculated and included in the structure-factor calculation with an isotropic ADP that was 1.2 or 1.5 times larger than that of bonded non-C or C atoms, respectively. Electron-density peaks higher than 0.3 e Å^{-3} were considered as solvent atoms, which were checked using the graphics program *TURBO-FRODO* (Roussel & Cambillau, 1991). A couple of solvent peaks with a distance of less than 2.5 Å were treated as disordered. The occupancy factors of solvent molecules were refined for atoms with no significant shift of atomic parameters and then fixed in subsequent calculations. Statistics of the structure refinement are given in Table 1.

2.4. Analysis of the rigid-body motion

The rigid-body motion of the xylanase II molecule was analyzed by the TLS model (Schomaker & Trueblood, 1968) to evaluate the thermal motion characteristics. This model represents rigid-body motion as a linear combination of translational motion (*T*), librational motion (*L*) and screw motion (*S*). Each term of the anisotropic displacement parameter, u_{ij}, is expressed as

$$u_{ij} = \sum G_{ijkl} L_{kl} + \sum H_{ijkl} S_{kl} + T_{ij},$$

where G_{ijkl} and H_{ijkl} are functions of the atomic coordinates. The tensor matrices L_{kl}, S_{kl} and T_{ij} were determined by the least-squares fit to observed u_{ij}. The centre of rotation was determined so that the S_{kl} matrix was symmetrical. Atomic

thermal motion consists of the rigid-body motion and internal motion, the latter of which is the fluctuation of the protein structure itself. The contribution from the internal motion, $u_{ij}^{\rm int}$, was estimated according to (Harata *et al.*, 1999)

$$u_{ij}^{\rm int} = u_{ij} - \left(k_{\rm L} \sum G_{ijkl} L_{kl} + k_{\rm T} T_{ij}\right),$$

where $k_{\rm L}$ and $k_{\rm T}$ are fractions of the librational and translational motions, respectively. The screw motion was not included in the calculation because its contribution was negligible.

3. Results

3.1. Molecular structure

The structure of the main-chain folding is shown in Fig. 1. The xylanase II molecule consists of one helix and 14 β-strands forming two bent-sheet structures. The backbone structure at 100 and 293 K is essentially the same as the structure of the monoclinic crystal (Törrönen *et al.*, 1994), on which the structure at 293 K can be superimposed with a mean difference of 0.5 Å between equivalent C^{α} atoms. The 100 K structure was fitted to the 293 K structure with a 0.4 Å mean deviation. However, no significant difference was observed between the structures determined at 290 and 293 K; the mean C^{α} difference was 0.04 Å. Fig. 2(*a*) shows a plot of the C^{α} difference between the structures at 100 and 293 K. Except for the N-terminal residue, the positional difference is less than 1.0 Å. Relatively large differences are observed in loop regions *A*, *B*, *C*, *D* and *T* which connect the β-strands. One obvious difference in the main-chain structure is disorder observed in the region Thr100–Ala102 at 293 K. This loop region forms a β-turn structure and two types of β-turns, types I and II, are located alternatively with equal occupancy. This conformational change between the two β-turns is caused by the 180° rotation of the peptide plane around the C^{α}—C bond of Thr100. Such a rotation is possible because of the flexible structure of the Gly101–Ala102 sequence. In contrast, only the type I β-turn is observed in the structure at 100 K. The structural change upon cooling suggests that the Thr100–Ala102 region is not in static disorder at 293 K, but fluctuates dynamically between the two conformations. The cooling to 100 K reduces the population of the type II β-turn, which may be less stable at a low temperature than the type I β-turn. The flash-freezing technique was applied to cool the crystal, but the heat conduction in the crystal was much slower than the shift of the equilibrium of the flip-flop motion between the two β-turn structures.

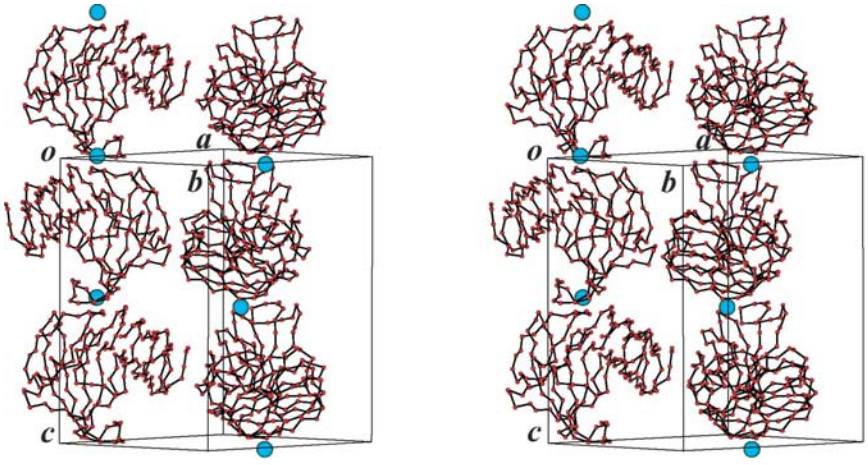

Figure 3
A stereoscopic view of the crystal packing of xylanase II molecules. Iodide ions are shown in blue.

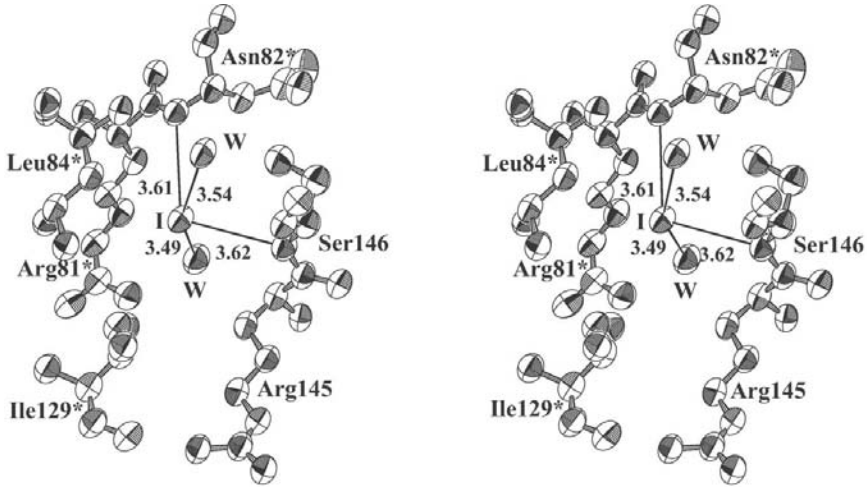

Figure 4
A stereoscopic view of hydrogen-bonding contacts of iodide ions drawn with *ORTEP*-III (Burnett & Johnson, 1996). Thermal ellipsoids are drawn with 30% probability. The asterisks denote amino-acid residues of an adjacent molecule.

The cooling to 100 K shrinks the crystal and the unit-cell volume is reduced to 95%. The shrinkage of the crystal should involve a change in the solvent structure in addition to a small shift of protein molecules. As a result, the conformation of some side chains exposed to solvent was affected. Most solvent molecules observed on the molecular surface were directly bound to protein molecules and they might move concertedly with the movement of the protein molecules or with the conformational change of the side-chain groups. The positions of the water molecules were compared between 100 and 293 K after the superposition of the protein molecules. Of the 208 water sites in the 293 K structure, 42 are within 0.3 Å of the corresponding water sites in the 100 K structure, while 115 sites are between 0.3 and 1.0 Å. Most of these water molecules are considered to be strongly bound to protein molecules by hydrogen bonds. In the

293 K structure, the hydroxyl groups of Ser36, Ser75 and Ser146 are disordered, each showing two alternate conformers. However, in the 100 K structure, alternate conformers are observed in the side chains of Gln34, Ser36, Asn38, Ser63, Ser65, Asn143, Thr168 and Met169. The increase in the number of disordered side-chain groups seems to be ascribed to the conformational change that occurs during cooling. The rapid loss of kinetic energy by flash-freezing prevented these side chains from reaching a single conformation that was stable at low temperature.

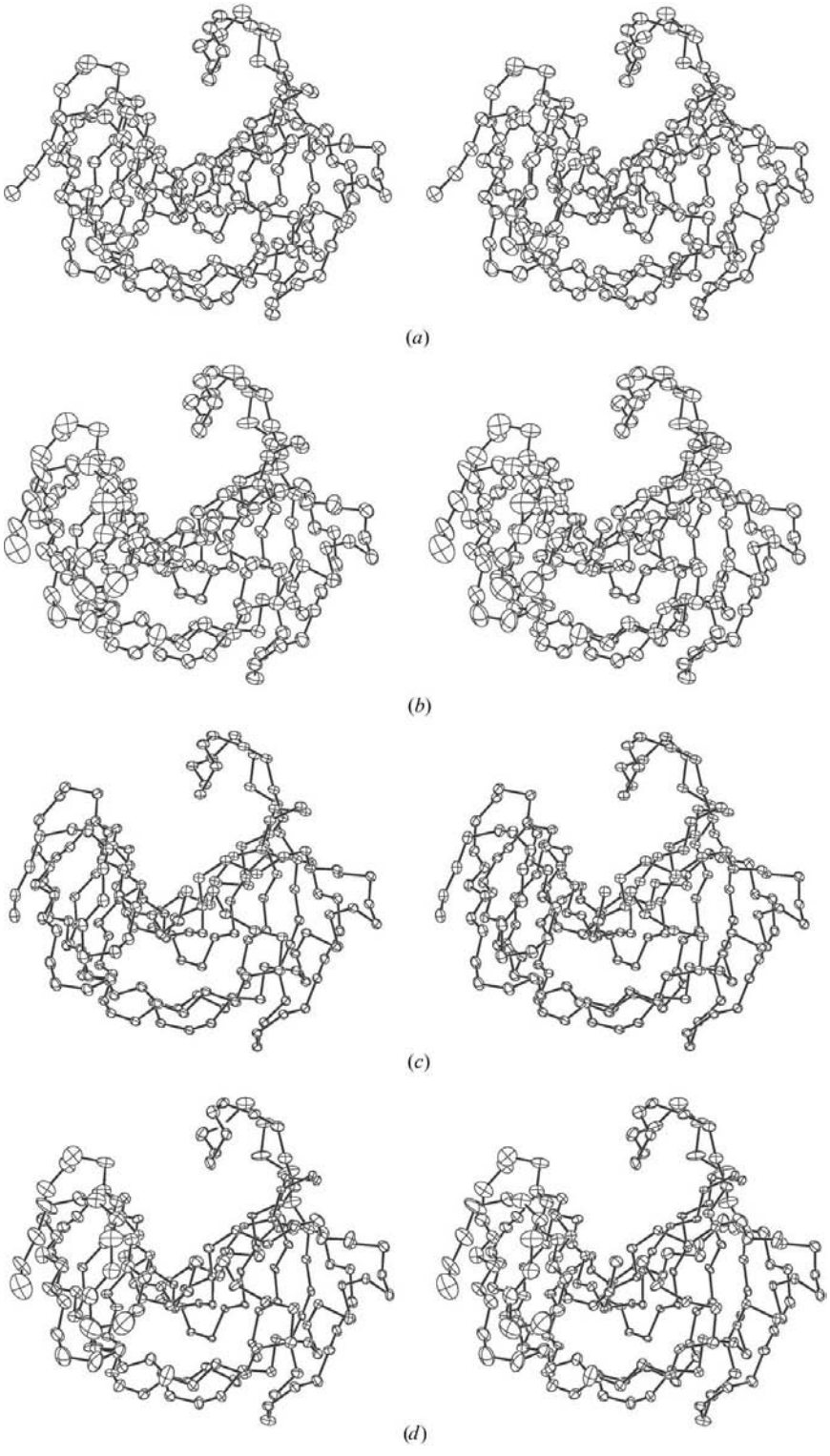

Figure 5
Comparison of anisotropic thermal motion of C^{α} atoms of the structures at 100 K (*a*) and 293 K (*b*) and the rigid-body motion (*c*) and internal motion (*d*) at 293 K. Thermal ellipsoids are drawn with 75% probability using *ORTEP*-III (Burnett & Johnson, 1996).

3.2. Crystal packing associated with the iodide linkage

As shown in Fig. 3, xylanase molecules are arranged along the *c* axis to form a helically extended polymeric chain. Adjacent molecules are connected by the iodide-mediated linkage that is formed between Ser146 and Asn82 of the adjacent molecule. The structure of the iodide-binding site is shown in Fig. 4. The main-chain N—H bonds of these two residues point to the iodide ion, thus forming N—H$\cdots$I$^-$ hydrogen bonds with N$\cdots$I$^-$ distances of 3.62 and 3.61 Å, which are similar to those observed in several protein crystal structures containing iodide ions (Steinrauf, 1998; Dauter *et al.*, 2000; Evans & Bricogne, 2003). Two water molecules are also hydrogen bonded to the iodide ion. Although the H atoms of these water molecules were not determined, the hydrogen bonding is indicated by the O$\cdots$I$^-$ distances of 3.49 and 3.54 Å, which fall in the range 3.37–3.64 Å observed in the crystal of the β-cyclodextrin complex with hydrogen iodide (Lindner & Saenger, 1982). In addition to the hydrogen-bonding contacts, the iodide ion is in van der Waals contact with the hydrophobic side-chain groups of Leu84 and Ile129. The H atoms of the alkyl side-chain groups are polarized and bear a positive charge. Therefore, the contact with these side-chain groups may be stabilized by a C—H$\cdots$I$^-$ interaction, which is expected to have an effect similar to the widely observed C—H$\cdots$O hydrogen bonds (Desiraju & Steiner, 1999) or C—H$\cdots\pi$ interactions (Nishio *et al.*, 1998). In the structure at 100 K, five minor binding sites of iodide ions were found. These iodide ions, which partially occupy the sites with occupancies of 0.58, 0.28, 0.22, 0.33 and 0.26, are also bound by hydrogen bonds but are not involved in the intermolecular protein–protein contacts. Two iodide ions are bound to main-chain peptide groups with N—H$\cdots$I$^-$ hydrogen bonds with Gly70 and Val123, while another iodide ion is chelated by the two guanidyl N—H groups of Arg119. The other two

Table 2
Summary of the analysis of atomic displacement parameters.

(*a*) Average u_{eqv} and e.s.d.s (Å^2). Average e.s.d.s. are given in parentheses.

Temperature (K)	100	293	290
Main-chain atoms	0.148 (0.006)	0.202 (0.011)	0.199(0.020)
All atoms	0.161 (0.017)	0.234 (0.021)	0.231(0.030)

(*b*) TLS analysis of xylanase structure at 293 K†. E.s.d.s are given in parentheses. The shift of the centre of rotation (*x*, *y*, *z*) from the centre of gravity in Å was (−4.13, −2.46, 0.32).

$T/10^{-3}$ (Å^2)	$L/10^{-6}$ (rad^2)	$S/10^{-4}$ (rad Å)
TLS matrices		
165 (2) 4 (1) −4 (1) 4 (1) 154 (2) 5 (1) −4 (1) 5 (1) 116 (2)	150 (13) 1 (5) −17 (5) 1 (5) 355 (16) 46 (6) −17 (5) 46 (6) 226 (14)	0 (1) 5 (1) 3 (1) 5 (1) −2 (1) 0 (1) 3 (1) 0 (1) 2 (1)
Eigenvalues		
(166, 153, 115)	(146, 370, 215)	

† Rigid-body parameters were determined by using a program developed in the authors' laboratory.

iodide ions are hydrogen bonded to a side-chain group of serine, asparagine or glutamine. In the 100 K structure, a sulfate ion is bound to the side chain of Asn19 by a direct hydrogen bond and by water-mediated hydrogen bonds with a phenolic hydroxyl group of Tyr17 and a carbonyl O atom of Val25. The side-chain groups of Trp51 and Lys58 of an adjacent molecule are also linked to the sulfate ion by water-mediated hydrogen-bond bridges. There are ten intermolecular hydrogen-bonding contacts between the protein molecules in the 293 K structure. All these contacts are conserved in the 100 K structure where, in addition, four direct hydrogen bonds are formed.

3.3. Analysis of thermal motion

A plot of the average u_{eqv} for each amino-acid residue is shown in Fig. 2(*b*). Atomic displacement parameters of the C^{α} atoms are represented by thermal ellipsoids, as shown in Fig. 5. A relatively large difference is observed in the loop regions connecting the β-strands, designated *A*, *B*, *C*, *D* and *T*, where the u_{eqv} values at 293 K (Fig. 5*a*) are considerably larger than those at 100 K (Fig. 5*b*). The rigid-body motion was evaluated to characterize the thermal fluctuation of the protein molecule at 293 K by using the TLS model (Fig. 5*c*). The results are summarized in Table 2. The contribution of the rigid-body motion to the atomic u_{eqv} was estimated to be 43.2% at 293 K. The r.m.s. amplitude of the translational motion is 0.38 Å, while the r.m.s. amplitude of the rotational motion is 0.89°, which corresponds to about a 0.2 Å shift in the atomic position on the molecular surface. Fig. 5(*d*) shows that the internal part of u_{ij} more clearly represents local fluctuations of the protein molecule than the observed u_{ij}. Because of the relatively small contribution of the rotational motion, the translational motion is predominant in the rigid-body motion. The principal axes of translational and rotational motions are shown in Fig. 6. The centre of rotation is shifted by 4.82 Å from the centre of gravity. In the translational motion, one axis is nearly parallel to the crystallographic *a* axis, while the plane made by the other two axes is rotated ∼20° around the *a* axis. The mean-square amplitude for the three principal axes (Table 2) indicates that the translational motion along the *c* axis is smaller than that along either the *a* or *b* axes. Therefore, it is plausible that the restriction imposed by the intermolecular linkage mediated by the iodide ion suppresses the translational vibration in the direction of the *c* axis.

4. Discussion

Sodium iodide or potassium iodide as an additive compound has proven useful for performing SAD or SIRAS phasing of diffraction data (Dauter *et al.*, 2000; Evans & Bricogne, 2003; Morth *et al.*, 2004). In the present structural study, we have shown that sodium iodide is also an effective additive for preparing a protein crystal with high diffraction quality. The crystal structure shows that the binding of the iodide ion stabilizes the molecular arrangement of this orthorhombic crystal, which did not grow in the presence of sodium chloride or sodium bromide. It is most likely that the iodide-mediated intermolecular hydrogen-bond linkage imposes a restriction on the molecular motion of proteins and suppresses the fluctuation in the molecular arrangement.

Xylanases belonging to the glycoside hydrolase family 11 are in the shape of a 'right hand', with the two β-sheets forming 'fingers' and the twisted part of the outer β-sheet and the α-helix forming a 'palm' (Törrönen *et al.*, 1994; Wakarchuk *et al.*, 1994; Krengel & Dijkstra, 1996). The long loop connecting the β-strands of residues 114–124 and 132–142 makes a 'thumb' (Fig. 1). The active site is constructed on the concave-like inner surface of the molecule, where two glutamic acid residues, Glu86 and Glu177 in xylanase II, reside at the active centre (Havukainen *et al.*, 1996; Sidhu *et al.*, 1999; Sabini *et al.*, 1999). The superposition of xylanase II molecules from four crystal structures indicates the open/closed movement of the active-site cleft formed by the 'thumb' and the lobe composed of the four 'fingers'. The mechanism underlying such a movement of local structures has been explained in terms of a hinge-like motion (Muilu *et al.*, 1998). However, the structural change upon substrate binding is small in the xylanases from *B. agaradhaerens* (Sabini *et al.*, 1999) and *B. circulans* (Sidhu *et al.*, 1999). A large loop shift of up to 1 Å has only been observed in the 'thumb' region in *B. circulans* xylanase. A relatively high mobility of the 'thumb' region has been also detected by NMR spectroscopy, although the whole structure of this xylanase is rigid on the picosecond to nanosecond timescale (Connelly *et al.*, 2000). In the present crystallographic analysis, the fluctuation of the local structures was evaluated by comparing anisotropic ADPs. The orthorhombic xylanase II structure drawn with thermal ellipsoids shows that the loop regions corresponding to the 'fingertips' have rela-

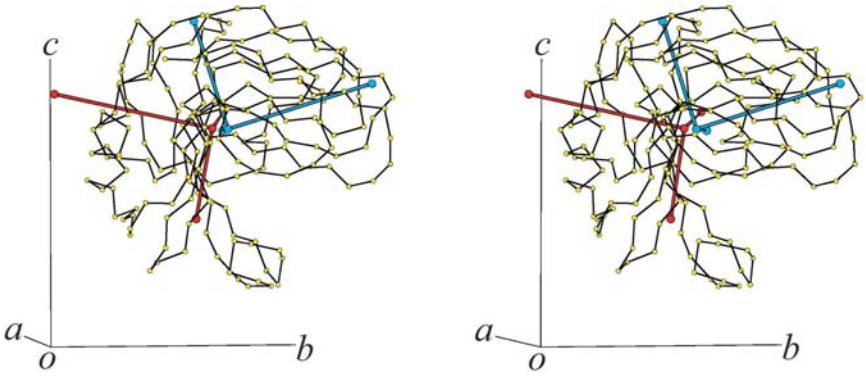

Figure 6
A stereoscopic drawing showing the principal axes of rigid-body rotation (red) and translation (blue). The principal axes of the translational motion are drawn from the centre of gravity of the molecule and those of the rotational motion are drawn from the centre of rotation, which is shifted by 4.82 Å from the centre of gravity. The directions of the lattice axes are shown by *a*, *b* and *c*.

tively large thermal motion at 293 K. Although the catalytic activity at this crystallization condition with pH 9.0 has not been reported (Joshi *et al.*, 2001; Turunen *et al.*, 2002), the high mobility of the local structures is considered intrinsic to, and important for, enzyme action. The distances of the $C^{\delta}-O^{\varepsilon 1}$ and $C^{\delta}-O^{\varepsilon 2}$ bonds in the catalytic residues are equivalent within estimated error: 1.253 (13) and 1.257 (13) Å in Glu86 and 1.255 (13) and 1.265 (17) Å in Glu177 in the structure at 100 K. These symmetrical carboxyl groups suggest that they are deprotonated (Wlodawer *et al.*, 2001). Since the active site is situated in the cleft formed by the 'thumb' and the four 'fingers', the large fluctuation of the 'fingertip' structures suggests that the

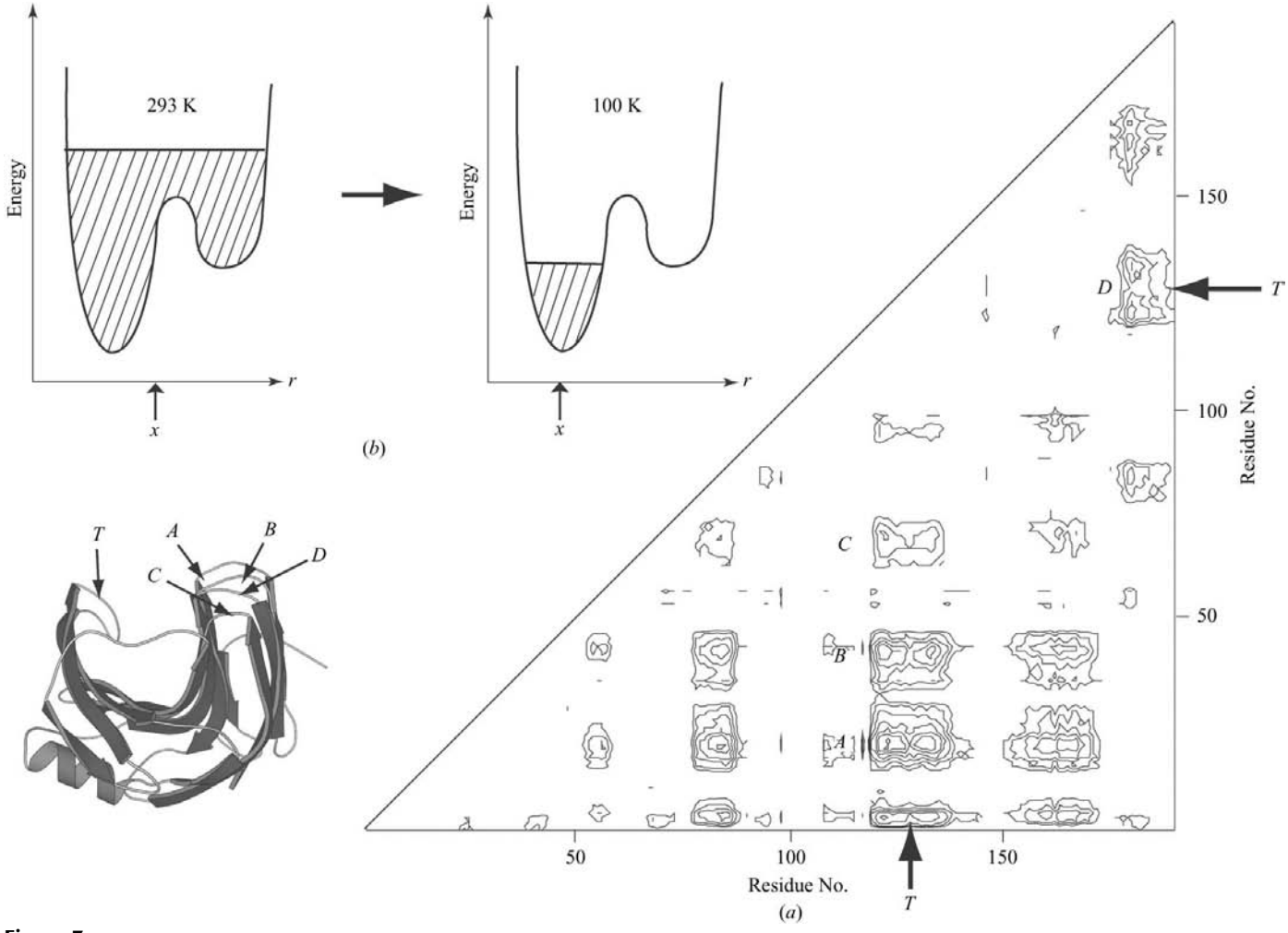

Figure 7
Distance difference map (*a*) showing the movement of C^{α} atoms between the structures at 100 and 293 K. The distance difference was calculated as the difference between the distances of C^{α} atoms as $\Delta r = r^{C_{\alpha}}(100\ \mathrm{K}) - r^{C_{\alpha}}(293\ \mathrm{K})$. Contours are drawn in the region from −0.4 to −1.8 Å with an interval of 0.2 Å. Loop regions corresponding to the 'fingertips' are denoted by *T* for the 'thumb' and *A*, *B*, *C* and *D* for the four 'fingers'. Schematic drawing of the energy landscape (*b*) shows the change of the population of the atomic position of the 'fingertip' regions induced by cooling from 293 to 100 K. An average position is denoted by *x*.

motion of these 'finger' regions is representative of the structural change associated with substrate binding or release of reaction products.

ADPs contain contributions from the rigid-body motion and internal motion, and internal motion is of biological interest in relation to the molecular function. Since rigid-body motion has been estimated to contribute around 50% to the ADPs in several protein crystals (Harata *et al.*, 1999; Harata & Kanai, 2002; Matoba & Sugiyama, 2003), it is necessary to correct for the effect of rigid-body motion in order to evaluate the internal fluctuation. The thermal fluctuation of the protein structure will be overestimated unless the rigid-body motion is considered in the analysis of the thermal motion. The analysis of the rigid-body motion of xylanase II, the results of which are shown in Fig. 5 and Table 2, demonstrates that the large thermal motion of the loop regions corresponding to the 'fingertips' cannot be interpreted in terms of the rigid-body motion, but could be assigned to the internal motion. The translational motion that contributes equally to all atoms in a protein molecule is predominant in the rigid-body motion. The effect of rotational motion is prominent on the edges or surface of the molecule and may be coupled with the hinge-like motion of the active site.

The mean amplitude of atomic vibration expressed in $u_{\rm eqv}^{1/2}$ corresponds to the radius of a sphere inside which the atom is found with a certain probability (Willis & Pryor, 1975; Burnett & Johnson, 1996). The $u_{\rm eqv}^{\rm int}$ value of the C^{α} atoms of the 'fingertip' regions in the xylanase II molecule is in the range 0.1–0.22 Å^2. Therefore, the atomic position in these loop regions fluctuates so much that there is only a 50% probability of finding a C^{α} atom in a sphere with a radius of about 0.6 Å. The comparison of the 293 K structure with the 100 K structure shows that the cleft becomes narrower by cooling to 100 K. The distance difference map (Fig. 7*a*) clearly shows that the distances between the 'thumb' (denoted by *T*) and the four fingers (denoted by *A*, *B*, *C* and *D*) are shorter by 0.8–1.7 Å at 100 K. An effect of the open/closed movement appears even at the bottom of the cleft, where the distance between the carboxyl C atoms of two catalytic residues, Glu86 and Glu177, is shortened by 0.45 Å at 100 K. This structural change, along with the prominent decrease in the magnitude of the ADP in the 100 K structure, suggests that the local structures forming the active-site cleft have a dynamic disorder that is too small to be resolved in the electron-density map. Relatively large ADPs in the 293 K structure may be attributable to the structure model that is fitted to the mean electron density of the fluctuating structure.

A dynamic disorder is observed in the structure of the region from Thr100 to Ala102, where the peptide group linking Thr100 and Gly101 is in a flip-flop disorder between the types I and II β-turn structures. These two conformers are clearly distinguished on the electron-density map at 293 K. The cooling to 100 K shifts the conformational equilibrium towards the type I β-turn. However, the 'fingers' forming the active-site cleft fluctuate in between unresolved local conformations at 293 K. As illustrated in Fig. 7(*b*), the fluctuating structure may fall into a most stable conformation upon cooling to 100 K. As a result, the cleft structure changes from the average of alternating conformers to a certain conformer. Such dynamic behaviour of the local structure cannot be detected in a single structure determined at either 100 or 293 K, but is revealed by a comparison of the structures determined at the two temperatures. If the disorder is static, the alternate conformers would be more clearly visible at low temperature (Walsh *et al.*, 1998), unless the cooling induces the conformational change.

This work was supported in part by the New Energy and Industrial Technology Development Organization (NEDO). We would like to thank Drs Naohiro Matsugaki, Noriyuki Igarashi, Mamoru Suzuki and Soichi Wakatsuki for their assistance with data collection at the Photon Factory, KEK.

References

Artymiuk, P. J., Blake, C. C. F., Grace, D. E. P., Oatley, S. J., Phillips, D. C. & Sternberg, M. J. E. (1979). *Nature (London)*, **280**, 563–568.
Bergfors, T. M. (1999). Editor. *Protein Crystallization: Techniques, Strategies and Tips.* La Jolla, CA, USA: International University Line.
Brünger, A. T., Adams, P. D., Clore, G. M., DeLano, W. L., Gros, P., Grosse-Kunstleve, R. W., Jiang, J.-S., Kuszewski, J., Nilges, M., Pannu, N. S., Read, R. J., Rice, L. M., Simonson, T. & Warren, G. L. (1998). *Acta Cryst.* D**54**, 905–921.
Burnett, M. N. & Johnson, C. K. (1996). *ORTEP-III: Oak Ridge Thermal Ellipsoid Plot Program for Crystal Structure Illustrations.* Report ORNL-6895, Oak Ridge National Laboratory, Oak Ridge, TN, USA.
Collaborative Computational Project, Number 4 (1994). *Acta Cryst.* D**50**, 760–763.
Connelly, G. P., Withers, S. G. & McIntosh, L. P. (2000). *Protein Sci.* **9**, 512–524.
Dauter, Z., Dauter, M. & Rajashankar, K. R. (2000). *Acta Cryst.* D**56**, 232–237.
DePristo, M. A., De Bakker, P. I. W. & Blundell, T. (2004). *Structure*, **12**, 831–838.
Desiraju, G. R. & Steiner, T. (1999). *The Weak Hydrogen Bond.* Oxford University Press.
Doucet, J. & Benoit, J. P. (1987). *Nature (London)*, **325**, 643–646.
Ducruix, A. & Giegé, R. (1999). Editors. *Crystallization of Nucleic Acids and Proteins.* Oxford University Press.
Evans, G. & Bricogne, G. (2003). *Acta Cryst.* D**59**, 1923–1929.
Evans, P. R. (1993). *Proceedings of the CCP4 Study Weekend. Data Collection and Processing*, edited by L. Sawyer, N. W. Isaacs & S. Bailey, pp. 114–122. Warrington: Daresbury Laboratory.
French, G. S. & Wilson, K. S. (1978). *Acta Cryst.* A**34**, 517–525.
Harata, K., Abe, Y. & Muraki, M. (1999). *J. Mol. Biol.* **287**, 347–358.
Harata, K. & Kanai, R. (2002). *Proteins*, **48**, 53–62.
Havukainen, R., Törrönen, A., Laitinen, T. & Rouvinen, J. (1996). *Biochemistry*, **35**, 9617–9624.
Henrissat, B. & Bairoch, A. (1993). *Biochem. J.* **293**, 781–788.
Joshi, M. D., Sidhu, G., Nielsen, J. E., Brayer, G. D., Withers, S. G. & McIntosh, L. P. (2001). *Biochemistry*, **40**, 10115–10139.
Kraulis, P. J. (1991). *J. Appl. Cryst.* **24**, 946–950.
Krengel, U. & Dijkstra, B. W. (1996). *J. Mol. Biol.* **263**, 70–78.
Lindner, K. & Saenger, W. (1982). *Carbohydr. Res.* **107**, 7–16.
McPherson, A. (1999). Editor. *Crystallization of Biological Macromolecules.* New York: CHSL Press.
Matoba, Y. & Sugiyama, M. (2003). *Proteins*, **51**, 453–469.
Merritt, E. A. (1999). *Acta Cryst.* D**55**, 1109–1117.
Morth, J. P., Feng, V., Perry, L. J., Svergun, D. I. & Tucker, P. A. (2004). *Structure*, **12**, 1595–1605.

Muilu, J., Törrönen, A., Perälylä, M. & Rouvinen, J. (1998). *Proteins*, **31**, 434–444.
Nishio, M., Hirota, M. & Umezawa, Y. (1998). *The CH/π Interaction.* New York: Wiley–VCH.
Otwinowski, Z. & Minor, W. (1997). *Methods Enzymol.* **276**, 307–326.
Petsko, G. A. (1996). *Nature Struct. Biol.* **3**, 565–566.
Roussel, A. & Cambillau, C. (1991). *Silicon Graphics Geometry Partners Directory*, p. 86. Mountain View, CA, USA: Silicon Graphics.
Sabini, E., Sulzenbacher, G., Dauter, M., Dauter, Z., Jørgensen, P. L., Schülein, M., Dupont, C., Davies, G. J. & Wilson, K. S. (1999). *Chem. Biol.* **6**, 483–492.
Sabini, E., Wilson, K. S., Danielsen, S., Schülein, M. & Davies, G. J. (2001). *Acta Cryst.* D**57**, 1344–1347.
Schmidt, A. & Lamzin, V. S. (2002). *Curr. Opin. Struct. Biol.* **12**, 698–703.
Schomaker, V. & Trueblood, K. N. (1968). *Acta Cryst.* B**24**, 63–76.
Sheldrick, G. M. (1997). *SHELXL97. Program for Crystal Structure Refinement.* University of Göttingen, Germany.
Sidhu, G., Withers, S. G., Nguyen, N. T., McIntosh, L. P., Ziser, L. & Brayer, G. D. (1999). *Biochemistry*, **38**, 5346–5354.
Steinrauf, L. K. (1998). *Acta Cryst.* D**54**, 767–779.
Sternberg, M. J. E., Grace, D. E. P. & Phillips, D. C. (1979). *J. Mol. Biol.* **130**, 231–253.
Teeter, M. M., Yamano, A., Stec, B. & Mohanty, U. (2001). *Proc. Natl Acad. Sci. USA*, **98**, 11242–11247.
Törrönen, A., Harkki, A. & Rouvinen, J. (1994). *EMBO J.* **13**, 2493–2501.
Törrönen, A. & Rouvinen, J. (1995). *Biochemistry*, **34**, 847–856.
Turunen, O., Vuorio, M., Fenel, F. & Leisola, M. (2002). *Protein Eng.* **15**, 141–145.
Usón, I., Sheldrick, G. M., de La Fortelle, E., Bricogne, G., Di Marco, S., Priestle, J. P., Grütter, M. G. & Mittl, P. R. E. (1999). *Structure*, **7**, 55–63.
Wakarchuk, W. W., Campbell, R. L., Sung, W. L., Davoodi, J. & Yaguchi, M. (1994). *Protein. Sci.* **3**, 467–475.
Walsh, M. A., Schneider, T. R., Sieker, L. C., Dauter, Z., Lamzin, V. & Wilson, K. S. (1998). *Acta Cryst.* D**54**, 522–546.
Willis, B. T. M. & Pryor, A. W. (1975). *Thermal Vibrations in Crystallography.* Cambridge University Press.
Wlodawer, A., Li, M., Gustchina, A., Dauter, Z., Uchida, K., Oyama, H., Goldfarb, N. E., Dunn, B. M. & Oda, K. (2001). *Biochemistry*, **40**, 15602–15611.
Zhang, X., Wozniak, J. A. & Matthews, B. W. (1995). *J. Mol. Biol.* **250**, 527–552.